

## Quantum Monte Carlo Diagonalization for many-fermion systems

Takashi Yanagisawa<sup>a,b</sup><sup>a</sup>*Condensed-Matter Physics Group, Nanoelectronics Research Institute,  
National Institute of Advanced Industrial Science and Technology (AIST),  
Central 2, 1-1-1 Umezono, Tsukuba 305-8568, Japan*<sup>b</sup>*CREST, Japan Science and Technology Agency (JST), Kawaguchi-shi, Saitama 332-0012, Japan*

(Dated: 2006; revised January 2007)

In this study we present an optimization method based on the quantum Monte Carlo diagonalization for many-fermion systems. Using the Hubbard-Stratonovich transformation, employed to decompose the interactions in terms of auxiliary fields, we expand the true ground-state wave function. The ground-state wave function is written as a linear combination of the basis wave functions. The Hamiltonian is diagonalized to obtain the lowest energy state, using the variational principle within the selected subspace of the basis functions. This method is free from the difficulty known as *the negative sign problem*. We can optimize a wave function using two procedures. The first procedure is to increase the number of basis functions. The second improves each basis function through the operators,  $e^{-\Delta\tau H}$ , using the Hubbard-Stratonovich decomposition. We present an algorithm for the Quantum Monte Carlo diagonalization method using a genetic algorithm and the renormalization method. We compute the ground-state energy and correlation functions of small clusters to compare with available data.

PACS numbers: 74.20.-z, 71.10.Fd, 75.40.Mg

## I. INTRODUCTION

The effect of the strong correlation between electrons is important for many quantum critical phenomena, such as unconventional superconductivity (SC) and the metal-insulator transition. Typical correlated electron systems are high-temperature superconductors[1–4], heavy fermions[5–8] and organic conductors[9]. Recently the mechanisms of superconductivity in high-temperature superconductors and organic superconductors have been extensively studied using various two-dimensional (2D) models of electronic interactions. Among them the 2D Hubbard model[10] is the simplest and most fundamental model. This model has been studied intensively using numerical tools, such as the Quantum Monte Carlo method [11–24], and the variational Monte Carlo method[25–33]. Recently, the two-leg ladder Hubbard model was also investigated with respect to the mechanism of high-temperature superconductivity[34–41].

The Quantum Monte Carlo (QMC) method is a numerical method employed to simulate the behavior of correlated electron systems. It is well known, however, that there are significant issues associated with the application to the QMC. First, the standard Metropolis (or heat bath) algorithm is associated with the negative sign problem. Second, the convergence of the trial wave function is sometimes not monotonic, and further, is sometimes slow. In past studies workers have investigated the possibility of eliminating the negative sign problem[21, 22, 24]. If the negative sign problem can be eliminated, the next

task would be to improve the convergence of the simulation method.

In this paper we present an optimization method based on Quantum Monte Carlo diagonalization (QMD or QMCD). The recent developments of high-performance computers have lead to the possibility of the simulation of correlated electron systems using diagonalization. Typically, and as in this study, the ground-state wave function is defined as

$$\psi = e^{-\tau H} \psi_0, \quad (1)$$

where  $H$  is the Hamiltonian and  $\psi_0$  is the initial one-particle state such as the Fermi sea. In the QMD method this wave function is written as a linear combination of the basis states, generated using the auxiliary field method based on the Hubbard-Stratonovich transformation; that is

$$\psi = \sum_m c_m \phi_m, \quad (2)$$

where  $\phi_m$  are basis functions. In this work we have assumed a subspace with  $N_{states}$  basis wave functions. From the variational principle, the coefficients  $\{c_m\}$  are determined from the diagonalization of the Hamiltonian, to obtain the lowest energy state in the selected subspace  $\{\phi_m\}$ . Once the  $c_m$  coefficients are determined, the ground-state energy and other quantities are calculated using this wave function. If the expectation values are not highly sensitive to the number of basis states, we can obtain the correct expectation values using an

extrapolation in terms of the basis states at the limit  $N_{states} \rightarrow \infty$ . However, a more reliable procedure must be employed when the change in the values at the limit is not monotonic. In this study results are compared to results obtained from an exact diagonalization of small clusters, such as  $4 \times 4$  and  $6 \times 2$  lattices.

In the following section, Section II, we briefly review the standard Quantum Monte Carlo simulation approach. In Section III a discussion of the Quantum Monte Carlo diagonalization, and an extrapolation method to obtain the expectation values, are presented. Section IV is a discussion of the optimization procedure which employs the diagonalization method. All the results obtained in this study are compared to the exact and available results of small systems in Section V. Finally, a summary of the work presented in this paper is presented in Section VI.

## II. QUANTUM MONTE CARLO METHOD

The method of Quantum Monte Carlo diagonalization lies in the QMC method. Thus it is appropriate to first outline the QMC method. The Hamiltonian is the Hubbard model containing on-site Coulomb repulsion and is written as

$$H = - \sum_{ij\sigma} t_{ij} (c_{i\sigma}^\dagger c_{j\sigma} + h.c.) + U \sum_j n_{j\uparrow} n_{j\downarrow}, \quad (3)$$

where  $c_{j\sigma}^\dagger$  ( $c_{j\sigma}$ ) is the creation (annihilation) operator of an electron with spin  $\sigma$  at the  $j$ -th site and  $n_{j\sigma} = c_{j\sigma}^\dagger c_{j\sigma}$ .  $t_{ij}$  is the transfer energy between the sites  $i$  and  $j$ .  $t_{ij} = t$  for the nearest-neighbor bonds. For all other cases  $t_{ij} = 0$ .  $U$  is the on-site Coulomb energy. The number of sites is  $N$  and the linear dimension of the system is denoted as  $L$ . The energy unit is given by  $t$  and the number of electrons is denoted as  $N_e$ .

In a Quantum Monte Carlo simulation, the ground state wave function is

$$\psi = e^{-\tau H} \psi_0, \quad (4)$$

where  $\psi_0$  is the initial one-particle state represented by a Slater determinant. For large  $\tau$ ,  $e^{-\tau H}$  will project out the ground state from  $\psi_0$ . We write the Hamiltonian as  $H = K + V$  where  $K$  and  $V$  are the kinetic and interaction terms of the Hamiltonian in Eq.(3), respectively. The wave function in Eq.(4) is written as

$$\psi = (e^{-\Delta\tau(K+V)})^M \psi_0 \approx (e^{-\Delta\tau K} e^{-\Delta\tau V})^M \psi_0, \quad (5)$$

for  $\tau = \Delta\tau \cdot M$ . Using the Hubbard-Stratonovich transformation[11, 42], we have

$$\begin{aligned} \exp(-\Delta\tau U n_{i\uparrow} n_{i\downarrow}) &= \frac{1}{2} \sum_{s_i = \pm 1} \exp(2as_i(n_{i\uparrow} - n_{i\downarrow}) \\ &\quad - \frac{1}{2}U\Delta\tau(n_{i\uparrow} + n_{i\downarrow})), \end{aligned} \quad (6)$$

for  $(\tanh a)^2 = \tanh(\Delta\tau U/4)$  or  $\cosh(2a) = e^{\Delta\tau U/2}$ . The wave function is expressed as a summation of the one-particle Slater determinants over all the configurations of the auxiliary fields  $s_j = \pm 1$ . The exponential operator is expressed as

$$\begin{aligned} (e^{-\Delta\tau K} e^{-\Delta\tau V})^M &= \frac{1}{2^{NM}} \sum_{\{s_i(\ell)\}} \prod_{\sigma} B_M^{\sigma}(s_i(M)) \\ &\quad \times B_{M-1}^{\sigma}(s_i(M-1)) \cdots B_1^{\sigma}(s_i(1)), \end{aligned} \quad (7)$$

where we have defined

$$B_{\ell}^{\sigma}(\{s_i(\ell)\}) = e^{-\Delta\tau K_{\sigma}} e^{-V_{\sigma}(\{s_i(\ell)\})}, \quad (8)$$

for

$$V_{\sigma}(\{s_i\}) = 2a\sigma \sum_i s_i n_{i\sigma} - \frac{1}{2}U\Delta\tau \sum_i n_{i\sigma}, \quad (9)$$

$$K_{\sigma} = - \sum_{ij} t_{ij} (c_{i\sigma}^\dagger c_{j\sigma} + h.c.). \quad (10)$$

The ground-state wave function is

$$\psi = \sum_m c_m \phi_m, \quad (11)$$

where  $\phi_m$  is a Slater determinant corresponding to a configuration  $m = \{s_i(\ell)\}$  ( $i = 1, \dots, N; \ell = 1, \dots, M$ ) of the auxiliary fields:

$$\begin{aligned} \phi_m &= \prod_{\sigma} B_M^{\sigma}(s_i(M)) \cdots B_1^{\sigma}(s_i(1)) \psi_0 \\ &\equiv \phi_m^{\uparrow} \phi_m^{\downarrow}. \end{aligned} \quad (12)$$

The coefficients  $c_m$  are constant real numbers:  $c_1 = c_2 = \dots$ . The initial state  $\psi_0$  is a one-particle state. If electrons occupy the wave numbers  $k_1, k_2, \dots, k_{N_{\sigma}}$  for each spin  $\sigma$ ,  $\psi_0$  is given by the product  $\psi_0^{\uparrow} \psi_0^{\downarrow}$  where  $\psi_0^{\sigma}$  is the matrix represented as[15]

$$\begin{pmatrix} e^{ik_1 \cdot r_1} & e^{ik_2 \cdot r_1} & \dots & \dots & e^{ik_{N_{\sigma}} \cdot r_1} \\ e^{ik_1 \cdot r_2} & e^{ik_2 \cdot r_2} & \dots & \dots & \dots \\ \cdot & \cdot & \cdot & \cdot & \cdot \\ e^{ik_1 \cdot r_N} & e^{ik_2 \cdot r_N} & \dots & \dots & \dots \end{pmatrix}. \quad (13)$$

$N_{\sigma}$  is the number of electrons for spin  $\sigma$ . In actual calculations we can use a real representation where the matrix elements are  $\cos(k_i \cdot r_j)$  or  $\sin(k_i \cdot r_j)$ . In the real-space representation, the matrix of  $V_{\sigma}(\{s_i\})$  is a diagonal matrix given as

$$V_{\sigma}(\{s_i\}) = \text{diag}(2a\sigma s_1 - U\Delta\tau/2, \dots, 2a\sigma s_N - U\Delta\tau/2). \quad (14)$$

The matrix elements of  $K_{\sigma}$  are

$$\begin{aligned} (K_{\sigma})_{ij} &= -t \quad i, j \text{ are nearest neighbors} \\ &= 0 \quad \text{otherwise.} \end{aligned} \quad (15)$$

$\phi_m^\sigma$  is an  $N \times N_\sigma$  matrix given by the product of the matrices  $e^{-\Delta\tau K_\sigma}$ ,  $e^{V_\sigma}$  and  $\psi_0^\sigma$ . The inner product is thereby calculated as a determinant[22],

$$\langle \phi_m^\sigma \phi_n^\sigma \rangle = \det(\phi_m^{\sigma\dagger} \phi_n^\sigma). \quad (16)$$

The expectation value of the quantity  $Q$  is evaluated as

$$\langle Q \rangle = \frac{\sum_{mn} \langle \phi_m Q \phi_n \rangle}{\sum_{mn} \langle \phi_m \phi_n \rangle}. \quad (17)$$

If  $Q$  is a bilinear operator  $Q_\sigma$  for spin  $\sigma$ , we have

$$\begin{aligned} \langle Q_\sigma \rangle &= \frac{\sum_{mn} \langle \phi_m^\sigma Q_\sigma \phi_n^\sigma \rangle \langle \phi_m^{-\sigma} \phi_n^{-\sigma} \rangle}{\sum_{mn} \langle \phi_m^\sigma \phi_n^\sigma \rangle \langle \phi_m^{-\sigma} \phi_n^{-\sigma} \rangle} \\ &= \frac{\sum_{mn} \langle \phi_m^\sigma Q_\sigma \phi_n^\sigma \rangle \det(\phi_m^{-\sigma\dagger} \phi_n^{-\sigma})}{\sum_{mn} \det(\phi_m^{\sigma\dagger} \phi_n^\sigma) \det(\phi_m^{-\sigma\dagger} \phi_n^{-\sigma})} \\ &= \sum_{mn} \frac{\det(\phi_m^{\sigma\dagger} \phi_n^\sigma) \det(\phi_m^{-\sigma\dagger} \phi_n^{-\sigma})}{\sum_{m'n'} \det(\phi_{m'}^{\sigma\dagger} \phi_{n'}^\sigma) \det(\phi_{m'}^{-\sigma\dagger} \phi_{n'}^{-\sigma})} \\ &\times \frac{\langle \phi_m^\sigma Q_\sigma \phi_n^\sigma \rangle}{\langle \phi_m^\sigma \phi_n^\sigma \rangle}. \end{aligned} \quad (18)$$

The expectation value with respect to the Slater determinants  $\langle \phi_m^\sigma Q_\sigma \phi_n^\sigma \rangle$  is evaluated using the single-particle Green's function[15, 22],

$$\frac{\langle \phi_m^\sigma c_{i\sigma} c_{j\sigma}^\dagger \phi_n^\sigma \rangle}{\langle \phi_m^\sigma \phi_n^\sigma \rangle} = \delta_{ij} - (\phi_n^\sigma (\phi_m^{\sigma\dagger} \phi_n^\sigma)^{-1} \phi_m^{\sigma\dagger})_{ij}. \quad (19)$$

In the above expression,  $P_{mn} \equiv \det(\phi_m^\sigma \phi_n^\sigma) \det(\phi_m^{-\sigma} \phi_n^{-\sigma})$  can be regarded as the weighting factor to obtain the Monte Carlo samples. Since this quantity is not necessarily positive definite, the weighting factor should be  $|P_{mn}|$ ; the resulting relationship is,

$$\begin{aligned} \langle Q_\sigma \rangle &= \sum_{mn} P_{mn} \langle Q_\sigma \rangle_{mn} / \sum_{mn} P_{mn} \\ &= \sum_{mn} |P_{mn}| \text{sign}(P_{mn}) \langle Q_\sigma \rangle_{mn} / \sum_{mn} |P_{mn}| \text{sign}(P_{mn}) \end{aligned} \quad (20)$$

where  $\text{sign}(a) = a/|a|$  and

$$\langle Q_\sigma \rangle_{mn} = \frac{\langle \phi_m^\sigma Q_\sigma \phi_n^\sigma \rangle}{\langle \phi_m^\sigma \phi_n^\sigma \rangle}. \quad (21)$$

This relation can be evaluated using a Monte Carlo procedure if an appropriate algorithm, such as the Metropolis or heat bath method, is employed[42]. The summation can be evaluated using appropriately defined Monte Carlo samples,

$$\langle Q_\sigma \rangle = \frac{\frac{1}{n_{MC}} \sum_{mn} \text{sign}(P_{mn}) \langle Q_\sigma \rangle_{mn}}{\frac{1}{n_{MC}} \sum_{mn} \text{sign}(P_{mn})}, \quad (22)$$

where  $n_{MC}$  is the number of samples. The sign problem is an issue if the summation of  $\text{sign}(P_{mn})$  vanishes within statistical errors. In this case it is indeed impossible to obtain definite expectation values.

### III. QUANTUM MONTE CARLO DIAGONALIZATION

#### A. Diagonalization

Quantum Monte Carlo diagonalization (QMD) is a method for the evaluation of  $\langle Q_\sigma \rangle$  without the *negative sign problem*. The configuration space of the probability  $\|P_{mn}\|$  in Eq.(22) is generally very strongly peaked. The sign problem lies in the distribution of  $P_{mn}$  in the configuration space. It is important to note that the distribution of the basis functions  $\phi_m$  ( $m = 1, 2, \dots$ ) is uniform since  $c_m$  are constant numbers:  $c_1 = c_2 = \dots$ . In the subspace  $\{\phi_m\}$ , selected from all configurations of auxiliary fields, the right-hand side of Eq.(17) can be determined. However, the large number of basis states required to obtain accurate expectation values is beyond the current storage capacity of computers. Thus we use the variational principle to obtain the expectation values.

From the variational principle,

$$\langle Q \rangle = \frac{\sum_{mn} c_m c_n \langle \phi_m Q \phi_n \rangle}{\sum_{mn} c_m c_n \langle \phi_m \phi_n \rangle}, \quad (23)$$

where  $c_m$  ( $m = 1, 2, \dots$ ) are variational parameters. In order to minimize the energy

$$E = \frac{\sum_{mn} c_m c_n \langle \phi_m H \phi_n \rangle}{\sum_{mn} c_m c_n \langle \phi_m \phi_n \rangle}, \quad (24)$$

the equation  $\partial E / \partial c_n = 0$  ( $n = 1, 2, \dots$ ) is solved for,

$$\sum_m c_m \langle \phi_n H \phi_m \rangle - E \sum_m c_m \langle \phi_n \phi_m \rangle = 0. \quad (25)$$

If we set

$$H_{mn} = \langle \phi_m H \phi_n \rangle, \quad (26)$$

$$A_{mn} = \langle \phi_m \phi_n \rangle, \quad (27)$$

the eigen equation is

$$Hu = EAu, \quad (28)$$

for  $u = (c_1, c_2, \dots)^t$ . Since  $\phi_m$  ( $m = 1, 2, \dots$ ) are not necessarily orthogonal,  $A$  is not a diagonal matrix. We diagonalize the Hamiltonian  $A^{-1}H$ , and then calculate the expectation values of correlation functions with the ground state eigenvector; in general  $A^{-1}H$  is not a symmetric matrix.

In order to optimize the wave function we must increase the number of basis states  $\{\phi_m\}$ . This can be simply accomplished through random sampling. For systems of small sizes and small  $U$ , we can evaluate the expectation values from an extrapolation of the basis of randomly generated states.

### B. Extrapolation

In Quantum Monte Carlo simulations an extrapolation is performed to obtain the expectation values for the ground-state wave function. If  $M$  is large enough, the wave function in Eq.(11) will approach the exact ground-state wave function,  $\psi_{exact}$ , as the number of basis functions,  $N_{states}$ , is increased. If the number of basis functions is large enough, the wave function will approach,  $\psi_{exact}$ , as  $M$  is increased. In either case the method employed for the reliable extrapolation of the wave function is a key issue in calculating the expectation values. If the convergence is fast enough, the expectation values can be obtained from the extrapolation in terms of  $1/N_{states}$ . Note that although the extrapolation in terms of  $1/M$ , or the time step  $\Delta\tau$ , has often been employed in QMC calculations, however, a linear dependence for  $1/M$  or  $\Delta\tau$  will not necessarily guarantee an accurate extrapolated result. The variance method was recently proposed in variational and Quantum Monte Carlo simulations, where the extrapolation is performed as a function of the variance. An advantage of the variance method lies in that linearity is expected in some cases[24, 43]:

$$\langle Q \rangle - Q_{exact} \propto v, \quad (29)$$

where  $v$  denotes the variance defined as

$$v = \frac{\langle (H - \langle H \rangle)^2 \rangle}{\langle H \rangle^2} \quad (30)$$

and  $Q_{exact}$  is the expected exact value of the quantity  $Q$ .

The following brief proof clearly shows that the energy in Eq.(30) varies linearly. If we denote the exact ground-state wave function as  $\psi_g$  and the excited states as  $\psi_i$  ( $i = 1, 2, \dots$ ), the wave function can be written as

$$\psi = a\psi_g + \sum_i b_i\psi_i, \quad (31)$$

where we assume that  $a$  and  $b_i$  are real and satisfy  $a^2 + \sum_i b_i^2 = 1$ . If it is assumed that  $H\psi_g = E_g\psi_g$  and  $H\psi_i = E_i\psi_i$ , the energy is found to be

$$\begin{aligned} E &= \langle H \rangle \\ &= a^2 \langle \psi_g H \psi_g \rangle + 2a \sum_i b_i \langle \psi_i H \psi_g \rangle + \sum_{ij} b_i b_j \langle \psi_i H \psi_j \rangle \\ &= a^2 E_g + \sum_{ij} b_i b_j \langle \psi_i H \psi_j \rangle \\ &= a^2 E_g + \sum_i b_i^2 E_i. \end{aligned} \quad (32)$$

The deviation of  $E$  from  $E_g$  is

$$\begin{aligned} \delta E &= E - E_g \\ &= (a^2 - 1)E_g + \sum_i b_i^2 E_i \\ &= b^2 (\langle E_i \rangle - E_g) \end{aligned} \quad (33)$$

where  $b^2 = 1 - a^2$  and  $\langle E_i \rangle = \sum_j b_j^2 E_j / \sum_j b_j^2$ . The variance  $v$  of  $H$  is also shown to be proportional to  $b^2$  if  $b^2$  is small. Since  $\langle H^2 \rangle = a^2 E_g^2 + b^2 \langle E_i^2 \rangle$  where  $\langle E_i^2 \rangle = \sum_j b_j^2 E_j^2 / \sum_j b_j^2$ ,  $v$  is evaluated as

$$v = C \left\{ (1 - b^2) \frac{\delta E}{E_g} - 2 \left( \frac{\delta E}{E_g} \right)^2 + \dots \right\}, \quad (34)$$

for a constant  $C$ . Hence if  $b$  is small it is found that

$$\frac{\delta E}{E_g} = \frac{v}{C} + O(v^2). \quad (35)$$

The other quantities can be found if  $Q_g = \langle \psi_g Q \psi_g \rangle$ , which leads to the result

$$\langle Q \rangle - Q_g = -b^2 Q_g + 2a \sum_i b_i \langle \psi_i Q \psi_g \rangle + \sum_{ij} b_i b_j \langle \psi_i Q \psi_j \rangle. \quad (36)$$

If  $Q$  commutes with  $H$ , and  $\psi_i$  are eigenstates of  $Q$ ,  $\langle Q \rangle - Q_g$  is proportional to  $b^2$ .

$$\langle Q \rangle - Q_g = -b^2 (Q_g - \langle Q_i \rangle), \quad (37)$$

where  $\langle Q_i \rangle = \sum_i b_i^2 \langle \psi_i Q \psi_i \rangle / \sum_i b_i^2$ ; thus  $\langle Q \rangle - Q_g \propto v$ . In the general case  $[H, Q] \neq 0$ ,  $\langle Q \rangle - Q_g$  is not necessarily proportional to  $b^2$ . However, if the matrix element  $\langle \psi_i Q \psi_g \rangle$  is negligible, we obtain

$$\begin{aligned} \langle Q \rangle - Q_g &= -b^2 Q_g + \sum_{ij} b_i b_j \langle \psi_i Q \psi_j \rangle \\ &= -b^2 (Q_g - \sum_{ij} b_i b_j \langle \psi_i Q \psi_j \rangle / \sum_i b_i^2). \end{aligned} \quad (38)$$

This shows that  $\langle Q \rangle - Q_g$  is proportional to the variance  $v$ . Thus, if  $\langle \psi_i Q \psi_g \rangle$  is small, we can perform an extrapolation using a linear fit to obtain the expectation values. We expect that this is the case for short-range correlation functions, since the local correlation may give rise to small effects in the orthogonality of  $\psi_i$  and  $\psi_g$ , i.e.  $\langle \psi_i \psi_g \rangle = 0$ . Hence the evaluations of local quantities will be much easier than for the long-range correlation functions.

## IV. OPTIMIZATION IN QUANTUM MONTE CARLO DIAGONALIZATION

### A. Simplest algorithm

The simplest procedure for optimizing the ground-state wave function is to increase the number of basis states  $\{\phi_m\}$  by random sampling. First, we set  $\tau$  and  $M$ , for example,  $\tau = 0.1, 0.2, \dots$ , and  $M = 20, 30, \dots$ . We denote the number of basis functions as  $N_{states}$ . We start with  $N_{states} = 100 \sim 300$  and then increase up to 2000 or 3000. This procedure can be outlined as follows:

A1. Generate the auxiliary fields  $s_i$  ( $i = 1, \dots, N$ )

in  $B_\ell^\sigma(\{s_i\})$  randomly for  $\ell = 1, \dots, M$  for  $\phi_m$  ( $m = 1, \dots, N_{states}$ ), and generate  $N_{states}$  basis wave function  $\{\phi_m\}$ .

A2. Evaluate the matrices  $H_{mn} = \langle \phi_m H \phi_n \rangle$  and  $A_{mn} = \langle \phi_m \phi_n \rangle$ , and diagonalize the matrix  $A^{-1}H$  to obtain  $\psi = \sum_m c_m \phi_m$ . Then calculate the expectation values and the energy variance.

A3. Repeat the procedure from A1 after increasing the number of basis functions.

For small systems this random method produces reliable energy results. The diagonalization plays an importance producing fast convergence.

Failure of this simple method sometimes occurs as the system size is increased. The eigenfunction of  $A^{-1}H$  can be localized when the off-diagonal elements are small, meaning that some components of  $c_m$  are large and others are negligible. A quotient of localization in the configuration space can be defined. For example, the summation of  $|c_m|^2$  except  $\phi_n$  with large  $c_n$  is a candidate for such property,

$$Q_{loc} = \sum'_m |c_m|^2, \quad (39)$$

where the prime indicates that the summation is performed excluding the largest  $c_n$ .  $Q_{loc}$  should approach 1 as the number of basis functions is increased. In the case of localization,  $Q_{loc} < 0.1$ , where to lower the energy is procedurally inefficient. In order to avoid the localization difficulty there are two possible procedures. First is to multiply  $\phi_m$  by  $B_\ell^\sigma(\{s_i\})$  to improve and optimize the basis wave function  $\phi_m$  further. Second, use a more effective method to generate new basis functions, explained further in the subsequent sections.

## B. Renormalization

The basis functions  $\{\phi_m\}$  multiplied by  $B_\ell^\sigma$  ( $\ell = M + 1, M + 2, \dots$ ) are improved to provide a lower ground state. Here the 'improvement' means the increase of  $\tau$  in Eq.(4) which is accomplished by increasing  $M$ . The matrix  $B_\ell^\sigma(\{s_i\})$  is given by a summation over  $2^N$  configurations of  $\{s_i\}$ . If we consider all of these configurations, the space required for basis functions becomes large. Thus, we should select several configurations or one configuration that exhibits the lowest energy. One procedure to choose such a state is the following:

R1. Multiply  $\phi_m$  by  $\prod_\sigma \exp(2a\sigma s_j n_{j\sigma} - \frac{1}{2}U\Delta\tau n_{j\sigma})$ , where we generate the auxiliary fields  $s_i(\ell)$  for  $\ell = M + 1$  and  $i = 1, \dots, N$  using random numbers. Then evaluate the ground state energy. If the energy is lower,  $\phi_m$  is defined as a new and improved basis function. If we have a higher energy,  $\phi_m$  remains unchanged. Repeat this procedure to lower the ground state energy twenty

to fifty times.

R2. Repeat above for  $m = 1, \dots, N_{states}$ .

R3. Multiply  $\phi_m$  by the kinetic operator  $e^{-\Delta\tau K_\uparrow}$  and  $e^{-\Delta\tau K_\downarrow}$ .

R4. Repeat from R1 and continue for  $\ell \rightarrow \ell + 1$ .

This method is referred to as the  $1/2^N$ -method in this paper since one configuration is chosen from  $2^N$  possible states. It is important to note that  $N_{states}$  remains unchanged. An alternative method has been proposed to renormalize  $\{\phi_m\}$  and is outlined as[24]:

R'1. Multiply  $\phi_m$  by  $\prod_\sigma \exp(2a\sigma s_j n_{j\sigma} - \frac{1}{2}U\Delta\tau n_{j\sigma})$  and evaluate the energy for  $s_j = 1$  and  $s_j = -1$ . We adopt  $s_j$  for which we have the lower energy.

R'2. Repeat this procedure for  $j = 1, \dots, N$  and determine the configuration  $\{s_j\}$  for  $\phi_m$ .

R'3. Multiply  $\phi_m$  by the kinetic operator  $e^{-\Delta\tau K_\uparrow}$  and  $e^{-\Delta\tau K_\downarrow}$ .

R'4. Repeat above for  $m = 1, \dots, N_{states}$  to improve  $\phi_m$ , and repeat from R1.

In this latter method the energy is calculated for the auxiliary field  $s_i = \pm 1$  at each site before making a selection. In the literature[24] this procedure is called the path-integral renormalization group (PIRG) method.

## C. Genetic algorithm

In order to lower the ground-state energy efficiently, we can employ a genetic algorithm[44] to generate the basis set from the initial basis set. One idea is to replace some parts of  $\{s_i(\ell)\}$  ( $i = 1, \dots, N; \ell = 1, \dots, M$ ) in  $\phi_n$  that has the large weight  $|c_n|^2$  to generate a new basis function  $\phi'_n$ . The new basis function  $\phi'_n$  obtained in this way is expected to also have a large weight and contribute to  $\psi$ .

Let us consider two basis functions  $\phi_m$  and  $\phi_n$  chosen from the basis set with a probability proportional to the weight  $|c_j|^2$  using uniform random numbers. For example, since  $\sum_{allj} |c_j|^2 = 1$ , we set the weight of  $\phi_\ell$  to occupy  $\sum_{j=1}^{\ell-1} |c_j|^2 < x < \sum_{j=1}^\ell |c_j|^2$  in the range  $0 < x < 1$ . If the random number  $r$  is within  $\sum_{j=1}^{m-1} |c_j|^2 < r < \sum_{j=1}^m |c_j|^2$ , we choose  $\phi_m$ , and  $\phi_n$  is similarly chosen. A certain part of the genetic data between  $\phi_m$  and  $\phi_n$  is exchanged, which results in two new basis functions  $\phi'_m$  and  $\phi'_n$ . We add  $\phi'_n$ , or  $\phi'_m$ , or both of them, to the set of basis functions as new elements. In this process every site is labeled using integers such as  $i = 1, \dots, N$ , and then we exchange  $s_i$  for  $i = L_1, L_1 + 1, \dots, L_1 + L_{exch} - 1$  where the number of  $s_i$  to be exchanged is denoted as  $L_{exch}$ .  $L_1$  can be determined using random numbers. We must also include a randomly generated new basis function as a mutation. Here we fix the numbers  $N_{states}$  and  $N_{step}$  before starting the Monte Carlo steps. For instance,

$N_{states} = 200$  and  $N_{step} = 200$ .  $N_{states}$  is increased as the Monte Carlo steps progress. We diagonalize the Hamiltonian  $A^{-1}H$  at each step when the  $N_{step}$  basis functions are added to the basis set in order to recalculate the weight  $|c_k|^2$  ( $k = 1, 2, \dots$ ). The procedure is summarized as follows:

- G1. Generate the auxiliary fields  $s_i(\ell)$  ( $i = 1, \dots, N$ ) randomly for  $\ell = 1, \dots, M$ . Generate  $N_{states}$  basis functions  $\{\phi_k\}$ . This is the same as A1.
- G2. Evaluate the matrices  $H_{mn} = \langle \phi_m H \phi_n \rangle$  and  $A_{mn} = \langle \phi_m \phi_n \rangle$ , and diagonalize the matrix  $A^{-1}H$  to obtain  $\psi = \sum_m c_m \phi_m$  and calculate the expectation values and the energy variance. This is the same as A2.
- G3. Determine whether a new basis function should be generated randomly or using the genetic method on the basis of random numbers. Let  $r_c$  be in the range  $0 < r_c < 1$ , for example,  $r_c = 0.9$ . If the random number  $r$  is less than  $r_c$ , a new basis function is defined using the genetic algorithm and the next step G4 is executed, otherwise generate the auxiliary fields  $\{s_i\}$  randomly and go to G6.
- G4. The weight of  $\phi_k$  is given as  $|c_k|^2$ . Choose two basis functions  $\phi_m$  and  $\phi_n$  from the basis set with a probability proportional to the weight  $|c_k|^2$ . Now we determine which part of the genetic code is exchanged between  $\phi_m$  and  $\phi_n$ . We choose  $\ell = \ell_0$  for  $1 \leq \ell \leq M$  using random numbers. We choose the sites  $j = L_1, \dots, L_2 = L_1 + L_{exch} - 1$  for a randomly chosen  $L_1$ .
- G5. Exchange the genetic code  $\{s_i(\ell)\}$  between  $\phi_m$  and  $\phi_n$  for  $\ell = \ell_0$  and  $j = L_1, \dots, L_2 + L_{exch} - 1$ . We have two new functions  $\phi'_m$  and  $\phi'_n$ . We adopt one or two of them as basis functions and keep the originals  $\phi_m$  and  $\phi_n$  in the basis set.
- G6. If the  $N_{step}$  basis functions are added up to the basis set after step G2, then repeat from step G2, otherwise repeat from step G3.

#### D. Hybrid optimization algorithm

In actual calculations it is sometimes better to use a hybrid of genetic algorithm and renormalization method. The concept to reach the ground-state wave function employed in this study is presented in Fig.1. There are two possible paths; one is to increase the number of basis functions using the genetic algorithm and the other is to improve each basis function by the matrix  $B_\ell(\{s_i\})$ . The path followed when the hybrid procedure is employed is the average of these two paths and is represented as the diagonal illustrated in Fig.1. Before step G6 in the genetic algorithm, the basis functions  $\phi_m$  are multiplied by  $B_\ell(\{s_i\})$  following the renormalization algorithm of the steps R1 to R3. Then we go to G6. The method is summarized as follows:

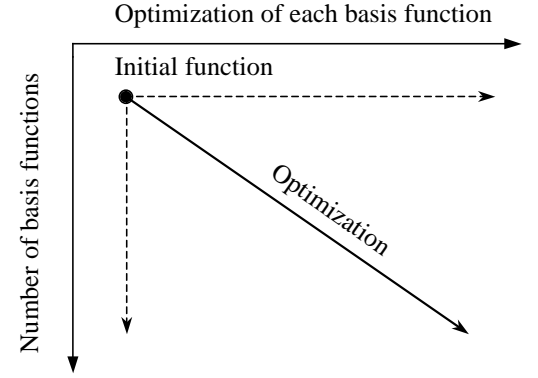


FIG. 1: Concept of optimization procedure. There are three approaches to reach the ground-state wave function. First is to increase the number of basis functions for fixed  $m$ . Second is to increase  $M$  multiplying each basis function by  $B_\ell(\{s_i\})$ . Third is the hybrid method of the previous two procedures.

- H1. Generate the auxiliary fields  $s_i(\ell)$  ( $i = 1, \dots, N$ ) randomly for  $\ell = 1, \dots, M$ . Generate  $N_{states}$  basis functions  $\{\phi_k\}$ .
- H2. Evaluate the matrices  $H_{mn} = \langle \phi_m H \phi_n \rangle$  and  $A_{mn} = \langle \phi_m \phi_n \rangle$ , and diagonalize the matrix  $A^{-1}H$  to obtain  $\psi = \sum_m c_m \phi_m$  and calculate the expectation values and the energy variance.
- H3. Determine whether a new basis should be generated randomly or using the genetic algorithm. Let  $r_c$  be in the range  $0 < r_c < 1$ . If the random number  $r$  is less than  $r_c$ , a new basis function is defined using the genetic algorithm and the next step is H4, otherwise generate the auxiliary fields  $\{s_i\}$  randomly and go to H6.
- H4. The weight of  $\phi_k$  is given as  $|c_k|^2$ . Choose two basis functions  $\phi_m$  and  $\phi_n$  from the basis set with a probability proportional to the weight  $|c_k|^2$ . Now we determine which part of the genetic code is exchanged between  $\phi_m$  and  $\phi_n$ . We choose  $\ell = \ell_0$  for  $1 \leq \ell \leq M$  using random numbers. We choose the sites  $j = L_1, \dots, L_2 = L_1 + L_{exch} - 1$  for a randomly chosen  $L_1$ .
- H5. Exchange the genetic code  $\{s_i\}$  between  $\phi_m$  and  $\phi_n$  for  $\ell = \ell_0$  and  $j$  determined in step H4. We have two new functions  $\phi'_m$  and  $\phi'_n$ . We adopt one or two of them as basis functions and keep the originals  $\phi_m$  and  $\phi_n$  in the basis set.
- H6. Multiply  $\phi_m$  by  $\prod_\sigma \exp(2a\sigma s_j n_{j\sigma} - \frac{1}{2}U\Delta\tau n_{j\sigma})$ , where we generate the auxiliary fields  $s_i(\ell)$  for  $\ell = M + 1$  and  $i = 1, \dots, N$  using random numbers. Then evaluate the ground state energy. If the energy is lower,  $\phi_m$  is defined as a new and improved basis function. If we have a higher energy,  $\phi_m$  remains unchanged. Repeat this procedure to lower the ground

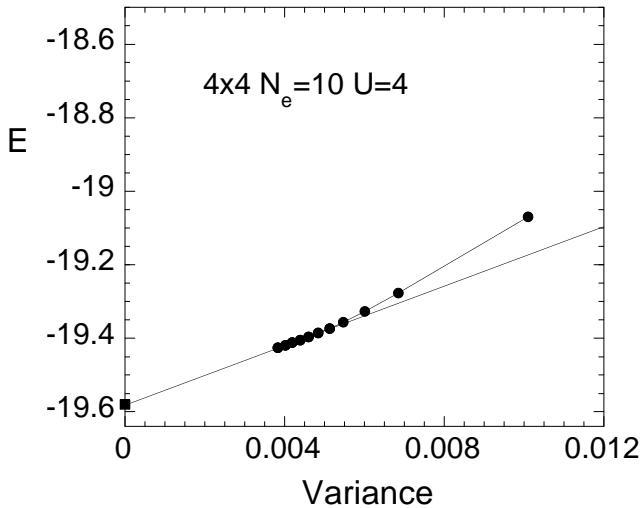


FIG. 2: Energy as a function of the variance for  $4 \times 4$ ,  $U = 4$  and  $N_e = 10$ . The square is the exact result. The data fit using a straight line using the least-square method as the variance is reduced. We started with  $N_{states} = 100$  (first solid circle) and then increase up to 2000.

state energy twenty to fifty times.

H7. Repeat above for  $m = 1, \dots, N_{states}$ .

H8. Multiply  $\phi_m$  by the kinetic operator  $e^{-\Delta\tau K_\uparrow}$  and  $e^{-\Delta\tau K_\downarrow}$ .

H9. If the  $N_{step}$  basis functions are added up to the basis set after step H2, then repeat from H2, otherwise repeat from step H3.

### E. Discussion on the Quantum Monte Carlo Diagonalization

The purpose of the QMD method is to calculate

$$\langle Q \rangle = \frac{\sum_{mn} c_m c_n \langle \phi_m Q \phi_n \rangle}{\sum_{mn} c_m c_n \langle \phi_m \phi_n \rangle}. \quad (40)$$

In an algorithm based on the Quantum Monte Carlo procedures, we evaluate the expectation values in the subspace  $\{\phi_i\}$ , selected from all the configurations of the auxiliary fields. From the data showing how the mean values  $\langle Q \rangle$  varies as the subspace is enlarged, we can estimate the exact value of  $\langle Q \rangle$  using an extrapolation. A devised algorithm may help us to perform the Quantum Monte Carlo evaluations efficiently. We have presented the genetic algorithm and the renormalization method. It may be possible to overcome the problem of localization in the subspace using this algorithm. In fact, the quotient  $Q_{loc}$  in Eq.(39) becomes nearly 1, i.e.  $Q_{loc} > 0.99$ , in the evaluations presented in the next section. For such a case, most of basis functions in the subspace give contributions to the mean values of physical quantities and the obtained results are certainly reliable.

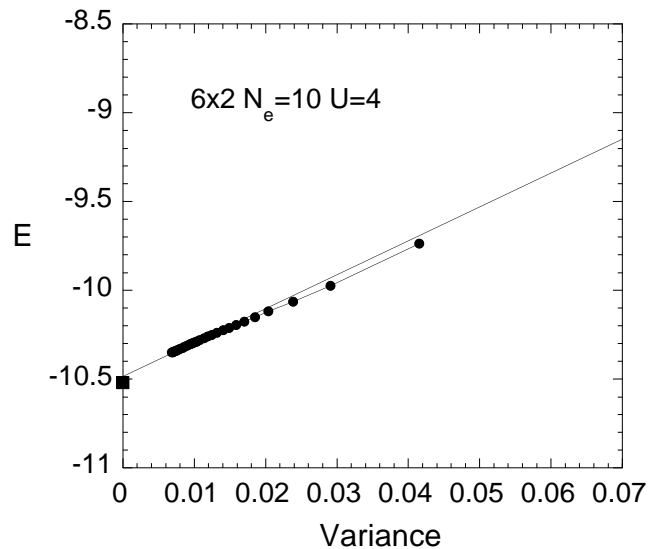


FIG. 3: Energy as a function of the variance for  $6 \times 2$   $N_e = 10$  and  $U = 4$ . The square is the exact value obtained using exact diagonalization.

## V. RESULTS

In this section, the results obtained using the QMD method are compared to the exact and available results. We investigate the small clusters (such as  $4 \times 4$  and  $6 \times 6$ ), the one-dimensional (1D) Hubbard model, the ladder Hubbard model, and the two-dimensional (2D) Hubbard model.

### A. Ground-state energy and correlation functions: check of the method

The results for the  $4 \times 4$ ,  $6 \times 2$  and  $6 \times 6$  systems are presented in Table I. The results are compared to the exact values and those available values obtained using the exact diagonalization, the quantum Monte Carlo method, the constrained path Monte Carlo method[22] and the variational Monte Carlo method for lattices with periodic boundary conditions. The expectation values for the ground state energy are presented for several values of  $U$ . The data include the cases for open shell structures where the highest-occupied energy levels are partially occupied by electrons. In the open shell cases the evaluations are sometimes extremely difficult. As is apparent from Table I, our method gives results in reasonable agreement with the exact values. The energy as a function of the variance is presented in Figs.2, 3 and 4. To obtain these results the genetic algorithm was employed to produce the basis functions except the open symbols in Fig.4. The  $4 \times 4$  where  $N_e = 10$  in Fig.2 is the energy for the closed shell case up to 2000 basis states. The other two figures are for open shell cases, where evaluations were performed up to 3000 states. Open symbols in Fig.4 indicate the en-

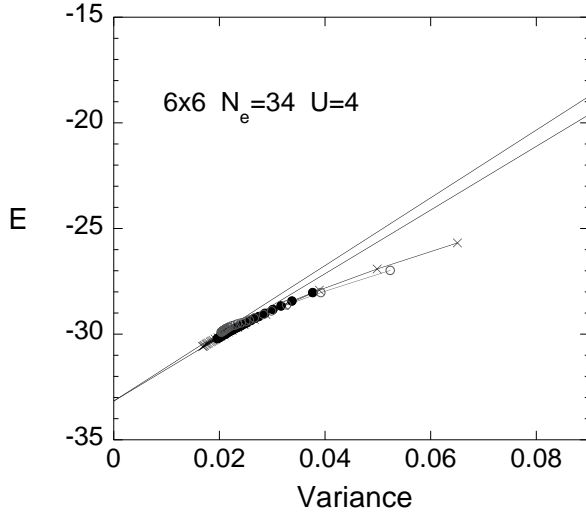


FIG. 4: Energy as a function of the variance  $v$  for  $6 \times 6$ , with the periodic boundary conditions. Solid circles and crosses are data obtained from the QMD method for two different initial configurations of the auxiliary fields. Gray open circles show results obtained from the  $1/2^N$ -renormalization method (PIRG) with 300 basis wave functions.

ergy obtained using the renormalization method ( $1/2^N$ -method) with 300 basis states. The results for the QMD and  $1/2^N$ -method (or PIRG) are quite similar as a function of the energy variance. In these cases  $Q_{loc}$  is close to 1;  $Q_{loc} \sim 0.99$ . As the variance is reduced, the data can fit using a straight line using the least-square method.

In Table I we have also included the VMC results for the  $\lambda$ -functions. The  $\lambda$ -functions are variational functions defined as follows. The Gutzwiller function is well known as

$$\psi_G = P_G \psi_0, \quad (41)$$

where  $P_G$  is the Gutzwiller projection operator,

$$P_G = \prod_j [1 - (1 - g)n_{j\uparrow}n_{j\downarrow}]. \quad (42)$$

$g$  is the parameter in the range  $0 \leq g \leq 1$ . The non-interacting wave function  $\psi_0$  is optimized by controlling the double occupancy  $\sum_j \langle n_{j\uparrow}n_{j\downarrow} \rangle$ . The further optimization of the Gutzwiller function can be obtained[48, 49],

$$\psi_\lambda^{(1)} = e^{-\lambda K} e^{-\alpha V} \psi_G, \quad (43)$$

$$\psi_\lambda^{(2)} = e^{-\lambda' K} e^{-\alpha' V} \psi_\lambda^{(1)}, \quad (44)$$

where  $K$  is the kinetic energy term and  $V$  is the on-site Coulomb interaction,

$$V = \sum_j n_{j\uparrow}n_{j\downarrow}, \quad (45)$$

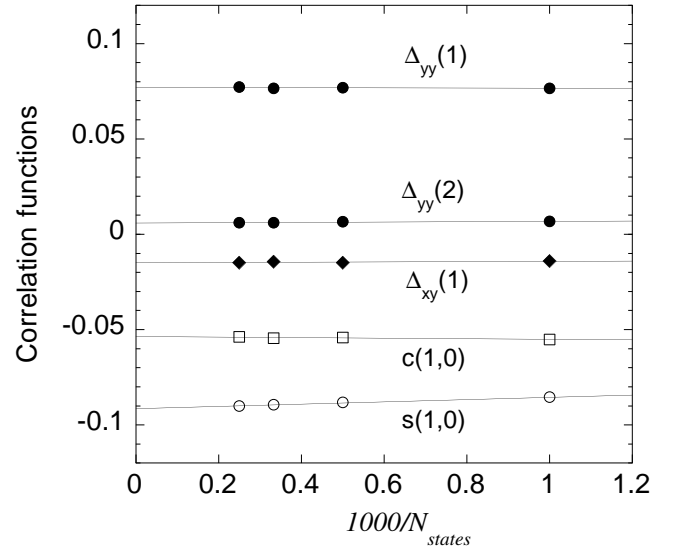


FIG. 5: Correlation functions obtained by QMD for  $4 \times 4$  lattice with  $N_e = 10$  and  $U = 4$  as a function of  $1/N_{states}$ .

where  $\lambda, \alpha, \lambda', \alpha'$  are variational parameters to be determined, to lower the ground-state energy.  $\alpha$  is related to  $g$  as  $\alpha = \log(1/g)$ . This type of wave function is referred to as  $\lambda$ -function in this paper. In our calculations the second level  $\lambda$ -function  $\psi_\lambda^{(2)}$  has given good results for the ground-state energy. If we perform an extrapolation as a function of the variance, we can obtain the correct expectation values as the QMD method. We must, however, determine variational parameters in the multi-parameter space by adjusting the values of the parameters to find a minimum. The advantage of the variational procedure is that the evaluations are stable even for large  $U/t$ , beyond the band width.

The correlation functions for the  $4 \times 4$  where  $N_e = 10$  and  $U = 4$  are presented in Table II. The exact diagonalization results are also provided. The correlation functions are defined as

$$S(\mathbf{q}) = \frac{1}{N} \sum_{ji} e^{i\mathbf{q} \cdot (\mathbf{R}_j - \mathbf{R}_i)} \langle (n_{j\uparrow} - n_{j\downarrow})(n_{i\uparrow} - n_{i\downarrow}) \rangle, \quad (46)$$

$$C(\mathbf{q}) = \frac{1}{N} \sum_{ji} e^{i\mathbf{q} \cdot (\mathbf{R}_j - \mathbf{R}_i)} (\langle n_j n_i \rangle - \langle n_j \rangle \langle n_i \rangle), \quad (47)$$

$$s(i, j) = \langle (n_{j\uparrow} - n_{j\downarrow})(n_{i\uparrow} - n_{i\downarrow}) \rangle, \quad (48)$$

$$c(i, j) = \langle n_j n_i \rangle - \langle n_j \rangle \langle n_i \rangle, \quad (49)$$

where  $n_j = n_{j\uparrow} + n_{j\downarrow}$  and  $\mathbf{R}_j$  denotes the position of the  $j$ -th site.  $\Delta_{\alpha\beta}$  is the pair correlation function,

$$\Delta_{\alpha\beta}(\ell) = \langle \Delta_\alpha^\dagger(i + \ell) \Delta_\beta(i) \rangle, \quad (50)$$

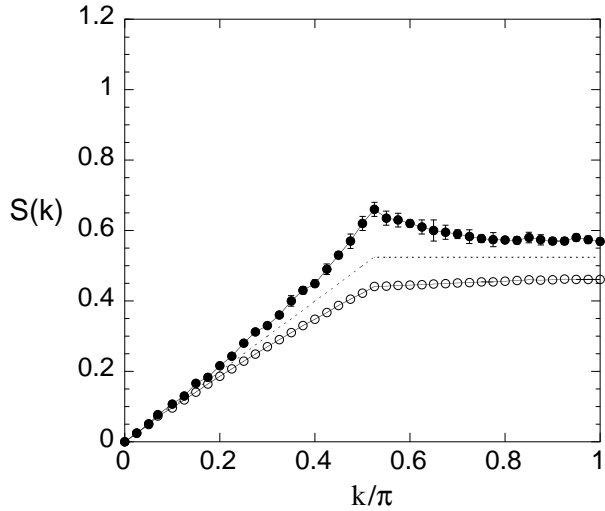


FIG. 6: Spin (solid circle) and charge (open circle) correlation functions obtained from the QMD method for the one-dimensional Hubbard model with 80 sites. The number of electrons is 66. We set  $U = 4$  and use the periodic boundary condition.

where  $\Delta_\alpha(i)$ ,  $\alpha = x, y$ , denote the annihilation operators of the singlet electron pairs for the nearest-neighbor sites:

$$\Delta_\alpha(i) = c_{i\downarrow}c_{i+\hat{\alpha}\uparrow} - c_{i\uparrow}c_{i+\hat{\alpha}\downarrow}. \quad (51)$$

Here  $\hat{\alpha}$  is a unit vector in the  $\alpha (= x, y)$ -direction. The agreement in this case is good for such a small system. The correlation functions are also dependent on the number of basis wave functions as shown in Fig.5. Since the fluctuation of the expectation values is small in this case, the extrapolation can be performed in terms of the  $1/N_{states}$ .

### B. 1D and Ladder Hubbard models

In this subsection we show the results for the one-dimensional (1D) Hubbard model and ladder Hubbard model. The ground state of the 1D Hubbard model is no longer Fermi liquid for  $U > 0$ . The ground state is insulating at half-filling and metallic for less than half-filling. The Fig. 6 is the spin and charge correlation functions,  $S(k)$  and  $C(k)$ , as a function of the wave number, for the 1D Hubbard model where  $N = 80$ . The  $2k_F$  singularity can be clearly identified where the dotted line is for  $U = 0$ . The spin correlation is enhanced and the charge correlation function is suppressed slightly because of the Coulomb interaction. The momentum distribution function  $n(k)$ ,

$$n(k) = \frac{1}{2} \sum_{\sigma} \langle c_{k\sigma}^\dagger c_{k\sigma} \rangle, \quad (52)$$

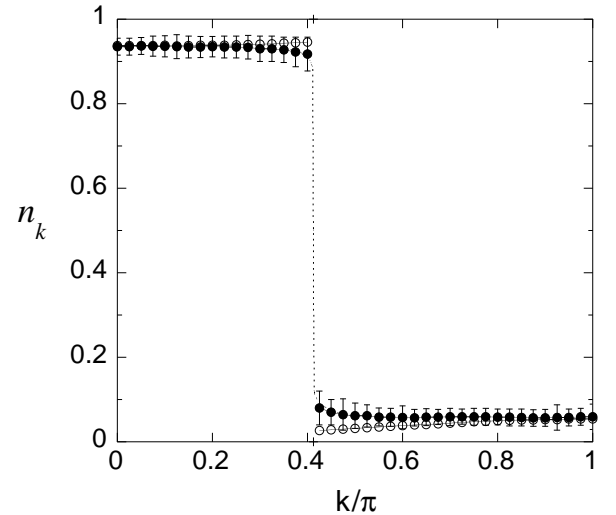


FIG. 7: Momentum distribution function obtained from the QMD method for the one-dimensional Hubbard model with 80 sites for the periodic boundary condition. The number of electrons is 66 and the Coulomb repulsion is  $U = 4$ . The dotted line is the guide given by  $n_k \sim 0.5 + 0.4|k - k_F|^{\eta-1}$  where  $\eta - 1 \sim 0.035$  which corresponds to  $K_\rho \sim 0.69$  using the formula  $\eta - 1 = (K_\rho + K_\rho^{-1})/4 - 1/2$ [50]. Open circles are the results obtained using the Gutzwiller function.

is presented in Fig.7 for the electron filling  $n = 0.825$ . Here  $c_{k\sigma}$  is the Fourier transform of  $c_{j\sigma}$ .  $n(k)$  in the metallic phase exhibits a singular behavior near the wave number  $k_F$ . The singularity close to  $k_F$  is consistent with the property of the Luttinger liquid[50, 51], although it is difficult to analyze the singularity in more detail using the Monte Carlo method. The Gutzwiller function gives the unphysical result that  $n(k)$  increases as  $k$  approaches  $k_F$  from above the Fermi surface.

In the ladder Hubbard model,

$$\begin{aligned} H_{ladder} = & -t \sum_{\ell=1,2} \sum_{j\sigma} (c_{\ell j\sigma}^\dagger c_{\ell j+1,\sigma} + \text{h.c.}) \\ & - t_d \sum_{j\sigma} (c_{1j\sigma}^\dagger c_{2j\sigma} + \text{h.c.}) \\ & + U \sum_{\ell=1,2} \sum_j c_{\ell j\uparrow}^\dagger c_{\ell j\uparrow} c_{\ell j\downarrow}^\dagger c_{\ell j\downarrow}, \end{aligned} \quad (53)$$

where  $t(t_d)$  is the intrachain (interchain) transfer energy. The ladder Hubbard model exhibits a spin gap at half-filling, and the charge gap is also possibly opened for large  $U > 0$  at half-filling. The existence of superconducting phase has been suggested for the Hubbard ladder using the DMRG method[38] and the VMC method[36].

The spin correlation function  $S(\mathbf{k})$  for the Hubbard ladder is presented in Fig.8, where  $U = 4$  and  $t_d = 1$ .

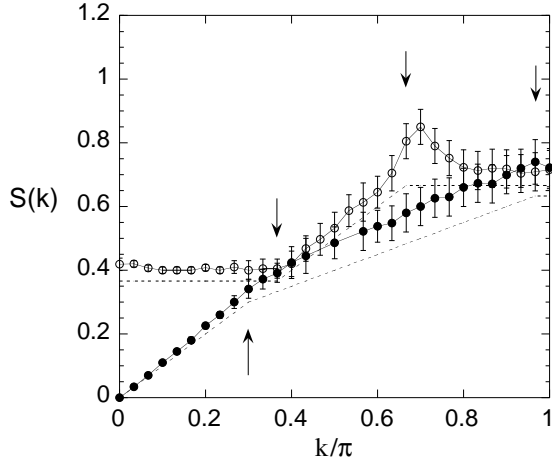


FIG. 8: Spin correlation function obtained from the QMD method for the ladder Hubbard model for  $60 \times 2$  sites with periodic boundary condition. The number of electrons is 80 and  $U = 4$ . The upper line is for the upper band and the lower line is for the lower band. Singularities are at  $k_{F1} - k_{F2}$ ,  $2k_{F2}$ ,  $k_{F1} + k_{F2}$  and  $2k_{F1}$  from left. The dotted lines are for  $U = 0$ .

$S(\mathbf{k})$  is defined as

$$S(\mathbf{k}) = \frac{1}{N} \sum_{i\ell, j\ell'} e^{i\mathbf{k} \cdot (\mathbf{R}_{i\ell} - \mathbf{R}_{j\ell'})} \langle (n_{\ell i \uparrow} - n_{\ell i \downarrow})(n_{\ell' j \uparrow} - n_{\ell' j \downarrow}) \rangle, \quad (54)$$

where  $\mathbf{R}_{i\ell}$  denotes the site  $(i, \ell)$  ( $\ell=1,2$ ). We use the convention that  $\mathbf{k} = (k, k_y)$  where  $k_y = 0$  and  $\pi$  indicate the lower band and upper band, respectively. There are four singularities at  $2k_{F1}$ ,  $2k_{F2}$ ,  $k_{F1} - k_{F2}$ , and  $k_{F1} + k_{F2}$  for the Hubbard ladder, where  $k_{F1}$  and  $k_{F2}$  are the Fermi wave numbers of the lower and upper band, respectively. They can be clearly identified as indicated by arrows in Fig.8.

The momentum distribution in Fig.9

$$n(\mathbf{k}) = \frac{1}{2N} \sum_{\sigma} \sum_{i\ell, j\ell'} e^{i\mathbf{k} \cdot (\mathbf{R}_{i\ell} - \mathbf{R}_{j\ell'})} \langle c_{\ell i \sigma}^{\dagger} c_{\ell' j \sigma} \rangle, \quad (55)$$

exhibits singularities at  $k_{F1}$  and  $k_{F2}$  where the results obtained from the Gutzwiller function are also shown for comparison. Here we used the same notation for  $\mathbf{k}$  and  $\mathbf{R}_{i\ell}$ . The unphysical property of  $n(\mathbf{k})$  near the Fermi wave numbers for the Gutzwiller function are remedied in the QMD method.

The pair correlation function,  $\Delta_{yy}(\ell)$  versus  $\ell$  was also evaluated to compare with the density matrix renormalization group (DMRG) method.  $\Delta_{yy}(\ell)$  is defined as

$$\Delta_{yy}(\ell) = \langle \Delta_y^{\dagger}(i + \ell) \Delta_y(i) \rangle \quad (56)$$

for

$$\Delta_y(i) = c_{1i\downarrow} c_{2i\uparrow} - c_{1i\uparrow} c_{2i\downarrow}. \quad (57)$$

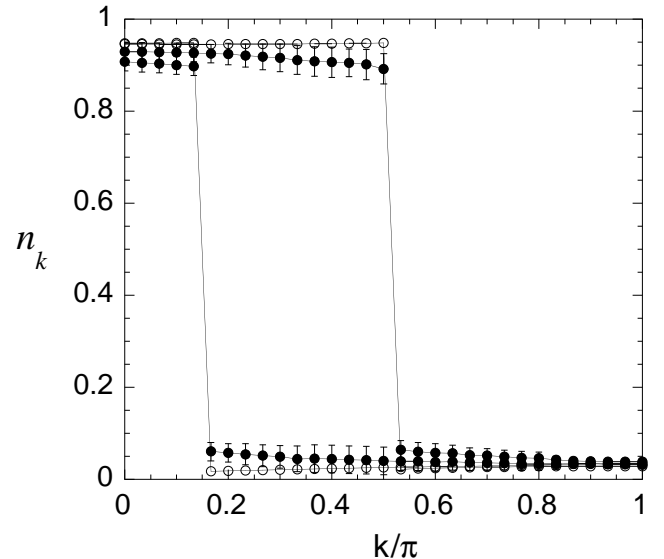


FIG. 9: Momentum distribution function obtained from the QMD method for the ladder Hubbard model for  $60 \times 2$  sites and periodic boundary condition. The number of electrons is 80 and  $U = 4$ .

$\Delta_{yy}(\ell)$  is the correlation function for the singlet pair on the rung. The results for  $\Delta_{yy}(\ell)$  are given in Fig.10 on the  $16 \times 2$  lattice for the open boundary condition, where the pair correlation functions  $\Delta_{yy}(\ell)$  were averaged over several pairs, for a distance  $\ell$ . The values  $U = 4$  and  $t_d = 1.4$  are predefined, and the electron filling was  $n = 0.875$ . The result obtained using the DMRG method is also provided for  $U = 8$ [38] for comparison. Since a large value of  $U$ , such as  $U = 8$ , is not easily accessed using the QMD method, we have presented the results for  $U = 4$ . The enhancement of the pair correlation function over the non-interacting case is clear and is consistent with the DMRG method.

It has been expected that the charge gap opens up as  $U$  turns on at half-filling for the Hubbard ladder model. In Fig.11 the charge gap at half-filling is shown as a function of  $U$ . The charge gap is defined as

$$\Delta_c = E(N_e + 2) + E(N_e - 2) - 2E(N_e), \quad (58)$$

where  $E(N_e)$  is the ground state energy for the  $N_e$  electrons. The charge gap in Fig.11 was estimated using the extrapolation to the infinite system from the data for the  $20 \times 2$ ,  $30 \times 2$ , and  $40 \times 2$  systems. The data are consistent with the DMRG method and suggest the exponentially small charge gap for small  $U$  or the existence of the critical value  $U_c$  in the range of  $0 \leq U_c < 1.5$ , below which the charge gap vanishes.

### C. 2D Hubbard model

The two-dimensional Hubbard model was also investigated in this study. The results are presented in the

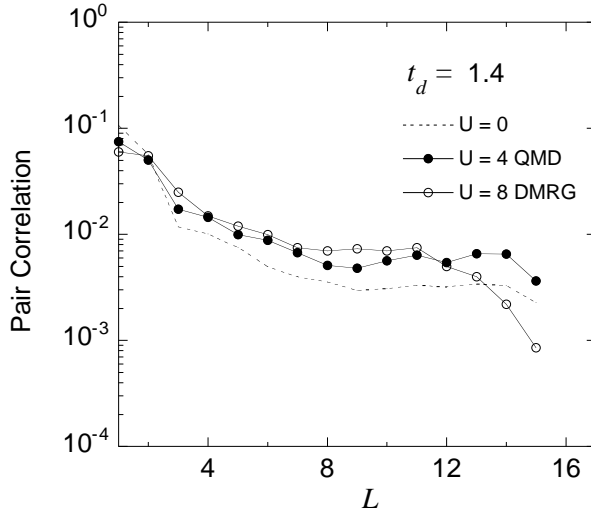


FIG. 10: Pair correlation function (solid circles) obtained using the QMD method for the ladder Hubbard model with  $16 \times 2$  sites where the boundary condition is open.  $U = 4$ ,  $t_d = 1.4$  and the electron filling is 0.875. The dashed line is the pair correlation function for  $U = 0$ . The open circles are the DMRG results from Ref.[38].

following discussion. An important issue is the antiferromagnetism at half-filling. The ground state is antiferromagnetic for  $U > 0$  because of the nesting due to the commensurate vector  $Q = (\pi, \pi)$ . The Gutzwiller function predicts that the magnetization

$$m = \left| \frac{1}{N} \sum_j (n_{j\uparrow} - n_{j\downarrow}) e^{iQ \cdot R_j} \right| \quad (59)$$

increases rapidly as  $U$  increases and approaches  $m = 1$  for large  $U$ . In Fig.12 the QMD results are presented for  $m$  as a function of  $U$ . The previous results obtained using the QMC method are plotted as open circles. The gray circles are for the  $\lambda$ -function VMC method and squares are the Gutzwiller VMC data. Clearly, the magnetization is reduced considerably because of the fluctuations, and is smaller than the Gutzwiller VMC method by about 50 percent.

The Fig. 13 is the momentum distribution function  $n(\mathbf{k})$ ,

$$n(\mathbf{k}) = \frac{1}{2} \sum_{\sigma} \langle c_{\mathbf{k}\sigma}^{\dagger} c_{\mathbf{k}\sigma} \rangle, \quad (60)$$

where the results for the Gutzwiller VMC and the QMD are indicated. The Gutzwiller function gives the results that  $n(k)$  increases as  $k$  approaches  $k_F$  from above the Fermi surface. This is clearly unphysical. This flaw of the Gutzwiller function near the Fermi surface is not observed for the QMD result.

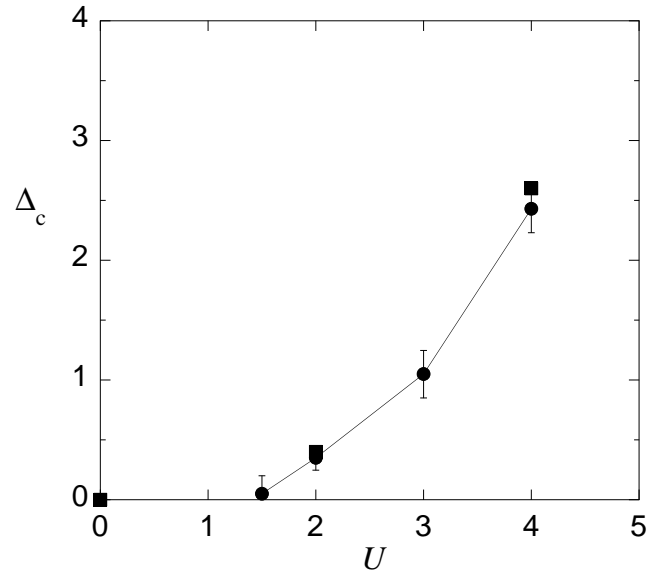


FIG. 11: Charge gap as a function of  $U$  for  $t_d = 1$  (circles). The DMRG results (squares) are provided for comparison[40].

## VI. SUMMARY

We have presented a Quantum Monte Carlo diagonalization method for a many-fermion system. We employ the Hubbard-Stratonovich transformation to decompose the interaction term as in the standard QMC method. We use this in an expansion of the true ground-state wave function. We have considered the truncated space of the basis functions  $\{\phi_m\}$  and diagonalize the Hamiltonian in this subspace. We can optimize the wave function by enlarging the subspace. The simplest way is to increase the number of basis functions by randomly generating auxiliary fields  $\{s_i\}$ . The wave function can be further

TABLE I: Ground state energy per site from the Hubbard model. The boundary conditions are periodic in both directions. The current results are presented under the column labeled QMD. The constrained path Monte Carlo (CPMC) and Path integral renormalization group (PIRG) results are from Refs.[22] and [24], respectively. The column VMC is the results obtained for the optimized variational wave function  $\psi_{\lambda}^{(2)}$  except for  $6 \times 2$  for which  $\psi_{\lambda}^{(1)}$  is employed. The QMC results are from Ref.[19]. Exact results are obtained using diagonalization[45].

Size	$N_e$	$U$	QMD	VMC	CPMC	PIRG	QMC	Exact
$4 \times 4$	10	4	-1.2237	-1.221(1)	-1.2238			-1.2238
$4 \times 4$	14	4	-0.9836	-0.977(1)	-0.9831			-0.9840
$4 \times 4$	14	8	-0.732(2)	-0.727(1)	-0.7281			-0.7418
$4 \times 4$	14	10	-0.656(2)	-0.650(1)				-0.6754
$4 \times 4$	14	12	-0.610(4)	-0.607(2)	-0.606			-0.6282
$6 \times 2$	10	2	-1.058(1)	-1.040(1)				-1.05807
$6 \times 2$	10	4	-0.873(1)	-0.846(1)				-0.8767
$6 \times 6$	34	4	-0.921(1)	-0.910(2)		-0.920	-0.925	
$6 \times 6$	36	4	-0.859(2)	-0.844(2)		-0.8589	-0.8608	

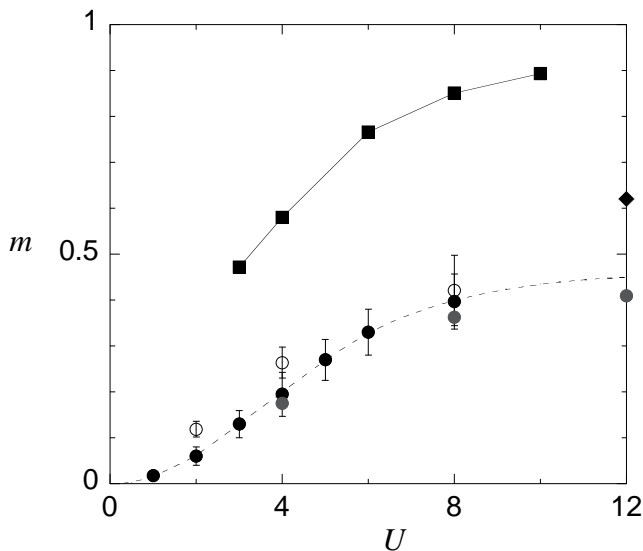


FIG. 12: Magnetization as a function of  $U$  for the half-filled Hubbard model after extrapolation at the limit of large  $N$ . Solid circles are the QMC results, and open circles are results obtained from the QMC method[12]. The squares are the Gutzwiller-VMC results[25] and gray solid circles show the 3rd  $\lambda$ -function ( $\psi_\lambda^{(3)}$ ) VMC results carried out on the  $8 \times 8$  lattice[49]. The diamond symbol is the value from the two-dimensional Heisenberg model where  $m = 0.615$ [46, 47].

improved by multiplying each  $\phi_m$  by  $B_\ell^\sigma$ . Although the matrix  $B_\ell^\sigma$  in Eq.(8) generates  $2^N$  new basis functions, we must select some states from them to keep the number of basis functions small. Within the subspace with the fixed number of basis functions, an extension of  $1/2^N$ -method to  $k/2^N$  method ( $k = 1, 2, \dots$ ) is also possible.

We have proposed a genetic-algorithm based method to generate the basis wave functions. The genetic algorithm is widely used in solving problems to find the optimized solution in the space of large configuration numbers. We make new basis functions from the functions with large weighting factors  $|c_n|^2$ . New functions produced in this way are expected to have large weighting factors. If the localization quotient  $Q_{loc}$  in Eq.(39) is not small, we can iterate the Monte Carlo steps without using the  $1/2^N$ -method.

We have computed the energy and correlation functions for small lattices to compare with published data. The results obtained in this study are consistent with the published data. In the case of the open shell structures, evaluations are difficult in general and the convergence is not monotonic. In this case the subspace of the basis functions must be large to obtain the expectation values from the extrapolation procedure.

As for the extrapolation, the expectation value  $\langle Q \rangle$  may approach  $Q_{exact}$  in a non-linear way,

$$\langle Q \rangle - Q_{exact} \propto (N_{states})^{-\theta} \quad (61)$$

for some exponent  $\theta$ . We must evaluate  $\theta$  to obtain  $Q_{exact}$ , from an extrapolation in terms of the  $N_{states}^{-1}$ . We

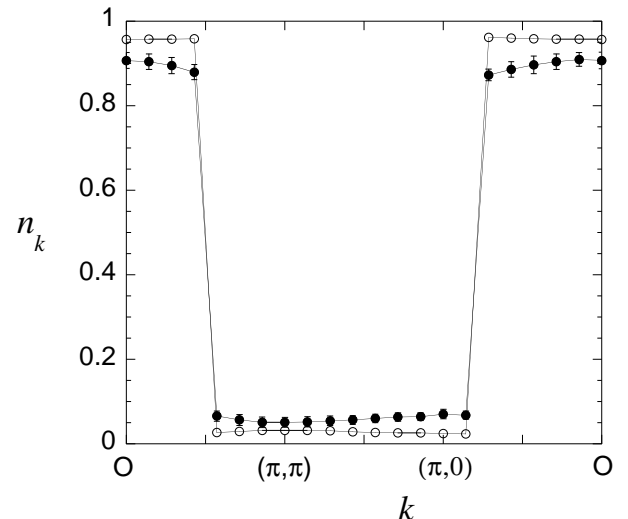


FIG. 13: Momentum distribution function for the  $14 \times 14$  lattice. Parameters are  $U = 4$  and  $N_e = 146$ . The boundary conditions are periodic in both directions. The results for the Gutzwiller function (open circle) are also provided.

may be able to use a derivative method where  $\theta$  is determined so that the derivative  $d\langle Q \rangle / dN_{states}$  approaches 0 as  $N_{states}$  increases. In this paper we adopted the recently proposed energy-variance method[24, 43]. For the energy and local quantities, we can expect  $\langle Q \rangle - Q_{exact} \propto v$  for the variance  $v$ . It is expected that the long-range correlations are not trivial to calculate since the orthogonality  $\langle \psi_i | Q | \psi_g \rangle \approx 0$  should hold for the ground state  $\psi_g$  and excited states  $\psi_i$ .

## VII. ACKNOWLEDGMENTS

We thank J. Kondo, K. Yamaji and S. Koikegami for helpful discussions.

## REFERENCES

- [1] E. Dagotto, Rev. Mod. Phys. 66, 763 (1994).
- [2] D. J. Scalapino, in *High Temperature Superconductivity- the Los Alamos Symposium - 1989 Proceedings*, edited by K. S. Bedell, D. Coffey, D. E. Deltzer, D. Pines, J. R. Schrieffer, (Addison-Wesley Publ. Comp., Redwood City, 1990) p.314.
- [3] P. W. Anderson, *The Theory of Superconductivity in the High- $T_c$  Cuprates* (Princeton University Press, Princeton, 1997).
- [4] T. Moriya and K. Ueda, Adv. Phys. 49, 555 (2000).
- [5] G. R. Stewart, Rev. Mod. Phys. 56, 755 (1984).

TABLE II: Correlation functions for the  $4 \times 4$  Hubbard model with periodic boundary conditions. Parameters are  $N_e = 10$  and  $U = 4$ . VMC indicates the variational Monte Carlo results obtained by  $\psi_\lambda^{(2)}$ . CPMC indicates the constrained path Monte Carlo results.

Correlation function	QMD	VMC	CPMC	Exact
$S(\pi, \pi)$	0.730(1)	0.729(2)	0.729	0.7327
$C(\pi, \pi)$	0.508(1)	0.519(2)	0.508	0.5064
$\Delta_{yy}(1)$	0.077(1)	0.076(1)		0.07685
$\Delta_{yy}(2)$	0.006(1)	0.006(1)		0.00624
$\Delta_{xy}(0)$	0.124(1)	0.120(2)		0.1221
$\Delta_{xy}(1)$	-0.015(1)	-0.015(1)		-0.0141
$s(0,0)$	0.529(1)			0.5331
$s(1,0)$	-0.091(1)			-0.0911
$c(0,0)$	0.329(1)			0.3263
$c(1,0)$	-0.0536(1)			-0.05394

[6] P. A. Lee, T. M. Rice, J. W. Serene, L. J. Sham and J. W. Wilkins, *Comments Cond. Matter Phys.* 12, 99 (1986).

[7] H. R. Ott, *Prog. Low Temp. Phys.* 11, 215 (1987).

[8] M. B. Maple, *Handbook on the Physics and Chemistry of Rare Earths* Vol. 30 (North-Holland, Elsevier, Amsterdam, 2000).

[9] T. Ishiguro, K. Yamaji and G. Saito, *Organic Superconductors* (Springer-Verlag, Berlin, 1998).

[10] J. Hubbard, *Proc. Roy. Soc. London, Ser A* 276, 238 (1963).

[11] J. E. Hirsch, *Phys. Rev. Lett.* 51, 1900 (1983).

[12] J. E. Hirsch, *Phys. Rev. B* 31, 4403 (1985).

[13] S. Sorella, E. Tosatti, S. Baroni, R. Car and M. Parrinell, *Int. J. Mod. Phys. B* 2, 993 (1988).

[14] S. R. White, D. J. Scalapino, R. L. Sugar, E. Y. Loh, J. E. Gubernatis, and R. T. Scalettar, *Phys. Rev. B* 40, 506 (1989).

[15] M. Imada and Y. Hatsugai, *J. Phys. Soc. Jpn.* 58, 3752 (1989).

[16] S. Sorella, S. Baroni, R. Car and M. Parrinello, *Europhys. Lett.* 8, 663 (1989).

[17] E. Y. Loh, J. E. Gubernatis, R. T. Scalettar, S. R. White, D. J. Scalapino, and R. L. Sugar, *Phys. Rev. B* 41, 9301 (1990).

[18] A. Moreo, D. J. Scalapino, and E. Dagotto, *Phys. Rev. B* 56, 11442 (1991).

[19] N. Furukawa and M. Imada, *J. Phys. Soc. Jpn.* 61, 3331 (1992).

[20] A. Moreo, *Phys. Rev. B* 45, 5059 (1992).

[21] S. Fahy and D. R. Hamann, *Phys. Rev. B* 43, 765 (1991).

[22] S. Zhang, J. Carlson and J. E. Gubernatis, *Phys. Rev. B* 55, 7464 (1997).

[23] S. Zhang, J. Carlson and J. E. Gubernatis, *Phys. Rev. Lett.* 78, 4486 (1997).

[24] T. Kashima and M. Imada, *J. Phys. Soc. Jpn.* 70, 2287 (2001).

[25] H. Yokoyama and H. Shiba, *J. Phys. Soc. Jpn.* 56, 1490 (1987); *ibid.* 56, 3582 (1987).

[26] C. Gros, R. Joynt, and T. M. Rice, *Phys. Rev. B* 36, 381 (1987).

[27] T. Nakanishi, K. Yamaji and T. Yanagisawa, *J. Phys. Soc. Jpn.* 66, 294 (1997).

[28] K. Yamaji, T. Yanagisawa, T. Nakanishi and S. Koike, *Physica C* 304, 225 (1998).

[29] T. Yanagisawa, S. Koike and K. Yamaji, *Phys. Rev. B* 64, 184509 (2001).

[30] T. Yanagisawa, S. Koike and K. Yamaji, *J. Phys.: Condens. Matter* 14, 21 (2002).

[31] T. Yanagisawa, S. Koike, S. Koikegami and K. Yamaji, *Phys. Rev. B* 67, 132408 (2003).

[32] T. Yanagisawa, M. Miyazaki and K. Yamaji, *J. Phys. Soc. Jpn.* 74, 835 (2005).

[33] M. Miyazaki, K. Yamaji and T. Yanagisawa, *J. Phys. Soc. Jpn.* 73, 1643 (2004).

[34] K. Yamaji and Y. Shimoi, *Physica C* 222, 349 (1994).

[35] K. Yamaji, Y. Shimoi and T. Yanagisawa, *Physica C* 235-240, 2221 (1994).

[36] S. Koike, K. Yamaji, and T. Yanagisawa, *J. Phys. Soc. Jpn.* 68, 1657 (1999); *ibid* 69, 2199 (2000).

[37] R. M. Noack, S. R. White, and D. J. Scalapino, *Physica C* 270, 281 (1996).

[38] R. M. Noack, N. Bulut, D. J. Scalapino, and M. G. Zacher, *Phys. Rev. B* 56, 7162 (1997).

[39] K. Kuroki, T. Kimura and H. Aoki, *Phys. Rev. B* 54, 15641 (1996).

[40] S. Daul and D. J. Scalapino, *Phys. Rev. B* 62, 8658 (2000).

[41] K. Sano, Y. Ono, and Y. Yamada, *J. Phys. Soc. Jpn.* 74, 2885 (2005).

[42] R. Blankenbecler, D. J. Scalapino, and R. L. Sugar, *Phys. Rev. D* 24, 2278 (1981).

[43] S. Sorella, *Phys. Rev. B* 64, 024512 (2001).

[44] D. E. Goldberg, *Genetic Algorithms in Search, Optimization and Machine Learning* (Addison-Wesley, Boston, 1989).

[45] A. Parola, S. Sorella, S. Baroni, R. Car, M. Parrinello and E. Tosatti, *Physica C* 162-164, 771 (1989).

[46] J. A. Riera and A. P. Young, *Phys. Rev. B* 39, 9697 (1989).

[47] M. Calandra Buonauro and S. Sorella, *Phys. Rev. B* 57, 11446 (1998).

[48] H. Ohtsuka, *J. Phys. Soc. Jpn.* 61, 1645 (1992).

[49] T. Yanagisawa, S. Koike and K. Yamaji, *J. Phys. Soc. Jpn.* 67, 3867 (1998); *ibid.* 68, 3608 (1999).

[50] H. J. Schulz, *Int. J. Mod. Phys. B* 5, 57 (1991).

[51] N. Kawakami and S.-K. Yang, *Phys. Lett. A* 148, 359 (1990).